Available online at www.sciencedirect.com

SciVerse ScienceDirect

Procedia CIRP 6 (2013) 438 – 443

www.elsevier.com/locate/procedia

The Seventeenth CIRP Conference on Electro Physical and Chemical Machining (ISEM)

Multiscale modeling of sinking-EDM with gaussian heat flux via user subroutine

Y.B. Guo[a,b]*, A. Klink[b], F. Klocke[b]

[a] Dept. of Mechanical Engineering, The University of Alabama, Tuscaloosa, AL 37587, USA

[b] Lab. for Machine Tools and Production Engineering, RWTH Aachen University, 52074 Aachen, Germany

* Corresponding author. Tel.: 1-205-348-2615; fax: +1-205-348-6419. *E-mail address*: yguo@eng.ua.edu.

Abstract

The EDM gap phenomena in the microscale time and space domains are very complex and challenging to analyze experimentally. However, the gap phenomena are critical to produce optimal surface integrity for superior performance of EDMed components. Nevertheless, the highly nonlinear transient dynamic process involving time/space-dependent plasma and heat flux has not been well understood. This work presents a multiscale finite element modeling for single discharging of ASP2023 tool steel to incorporate the plasma-induced time/space-dependent Gaussian heat flux via a user subroutine. The long-standing numerical singularity of heat flux in EDM modeling is solved using the innovative functions of discharge current. The effects of discharge duration and current on temperature profiles, crater formation, and dimensions are investigated. The basic mechanisms of superheating and melting can be successfully predicted. In addition, melting front recedes at long discharge duration, while melting front advances at high discharge current.

Keywords: EDM; gap phenomena; heat flux; multiscale modeling

1. Introduction

EDM is a competitive manufacturing process to machine difficult-to-cut materials such as hardened steels, super alloys, cemented carbides, and conductive ceramics. However, the thermal nature of EDM is expected to damage surface integrity. The potential damage on surface integrity depends on the levels of temperatures during an EDM process. Since the process-induced surface integrity has a significant impact on functions of the EDMed components, a fundamental understanding on EDM mechanism is critical to select optimal machining conditions. However, the complex EDM gap phenomena [1], involving multiphysics such as gas discharge, conduction and breakdown in liquids, and underwater explosion, have not been well understood. EDM occurs over microsecond time domain (several μs – 100 μs) and micrometer space (< 100 μm) filled with dielectric liquid, and involve evaporation and melting of materials in high gradients, thus making experimental measurement even observation extremely difficult.

Finite element analysis (FEA) provides a suitable tool to study the multiscale and multiphysics EDM phenomena. Despite some efforts have been pursued to predict temperatures in an EDM process [2-6], multiphysics EDM has not been well understood in the studies. The major difficulty is that EDM is a highly nonlinear transient dynamic process involving time-dependent plasma and time/space-dependent heat flux (radius and magnitude). DiBitonto et al. assumed a point heat source model (PHSM) of cathode erosion [7], expanding-circle heat source model (ECHSM) for anode erosion [8], and the variable mass, cylindrical plasma model (VMCPM) [9]. However, an equivalent uniform heat flux was used in these models. The singularity issue of heat flux at nanosecond discharge is inherent in the numerical calculations [8]. Xia et al. [10] found that the boundary conditions: heat source diameter, heat flux

doi:10.1016/j.procir.2013.03.047

distribution, and timing of metal removal, exert a significant influence on the calculation results. Unfortunately, however, determining the boundary conditions is still a controversial issue.

An insight on the electrical discharge mechanism remains a challenging problem. The objectives of this work are in several fold: (1) Develop a multiscale (time and space) modeling procedure to incorporate the plasma-induced heat flux and heat transfer in workpiece; (2) Model the time/space-dependent Gaussian heat flux; (3) Solve the long-time standing singularity issue of heat flux in EDM modeling; and (4) Shed light on the fundamental mechanism of EDM process.

2. *Multiscale FEA modeling procedure*

2.1 Simulation procedure

A 3D semi-infinite model was used to simulate single EDM discharge of ASP23 tool steel. The temperature-dependent physical and mechanical properties of the powder metallurgical work material are in Tables 1-2. Since EDM is a highly transient dynamic process that induces very high temperatures, an explicit simulation seems to be a reasonable approach to simulate the process. However, an implicit approach will ensure simulation convergence without sacrificing simulation cost. In addition, the time/space-dependent Gaussian heat flux can only be coded through a user subroutine via Abaqus/standard [11]. A series of simulations, Table 3, were performed in order to evaluate the influence of important process parameters.

Table 1. Physical properties of ASP2023 tool steel*

Material constant	Temperature (ºC)		
	20	400	600
Density (Kg/m^3)	8050	7940	7875
Modulus of elasticity (GPa)	230	205	184
Coefficient of thermal expansion (20 ºC, per ºC)	--	12.1 $\times 10^{-6}$	12.7 $\times 10^{-6}$
Thermal conductivity (W/m ºC)	24	28	27
Specific heat (J/kg ºC)	420	510	600
Melting temperature (ºC)	1353		

*62 HRc, hardened 1180ºC and tempered 3×1 h at 560ºC

Table 2. Mechanical properties of ASP2023 tool steel

Material constant	Temperature (°C)		
	20	400	600
Density (Kg/m^3)	8050	7940	7875
Modulus of elasticity (GPa)	230	205	184
Thermal expansion coefficient (m/°C)	1.11E-05	1.21E-05	1.27E-05
Thermal conductivity (W/m °C)	-	28	27
Specific heat (J/Kg °C)	420	510	600
Stress (GPa), plastic strain	(1.84, 0) (2.2, 4.35e-4) (2.5, 1.13e-3) (2.7, 2.40e-3)	NA	NA

Table 3. Sinking-EDM simulation conditions

Case #	EDM process parameters			Current $I(t)$ parameter			
	U (V)	T_e (µs)	I (A)	K_1	K_2	K_3	b
1	20	10	30	1.92E+21	30	1.20E+08	1.20E+03
2	20	25	30	1.23E+20	30	4.80E+07	1.20E+03
3	20	50	30	1.54E+19	30	2.40E+07	1.20E+03
4	20	75	30	4.55E+18	30	1.60E+07	1.20E+03
5	20	100	30	1.92E+18	30	1.20E+07	1.20E+03
6	20	50	10	5.12E+18	10	8.00E+06	4.00E+02
7	20	50	20	1.02E+19	20	1.60E+07	8.00E+02
8	20	50	30	1.54E+19	30	2.40E+07	1.20E+03
9	20	50	40	2.05E+19	40	3.20E+07	1.60E+03
10	20	50	50	2.56E+19	50	4.00E+07	2.00E+03

2.2 Mesh and assumptions

The 3D mesh in Fig. 1 is a quarter cylinder consisted of axisymmetric CAX3T and CAX4T finite elements and semi-infinite CINAX4 elements. Since it is a single discharge simulation, only one quarter mesh was modeled with X-/Z-axis symmetry. The mesh allows for a comprehensive analysis of 3D temperature fields in the subsurface while minimizing computation time. Temperature is a degree-of-freedom of the selected heat transfer elements. The initial temperature of the workpiece is 293 K. The mesh had four regions with adaptive mesh densities. The region where the heat flux was applied contains a fine mesh of 0.5 µm cubic elements, which provides high spatial resolution for spatial convergence.

A few assumptions were made for the simulations:

- The temperature-dependent material properties are homogeneous and isotropic.
- A single spark discharge is simulated.
- The heat transfer mode is conduction, while radiation and convection are ignored.

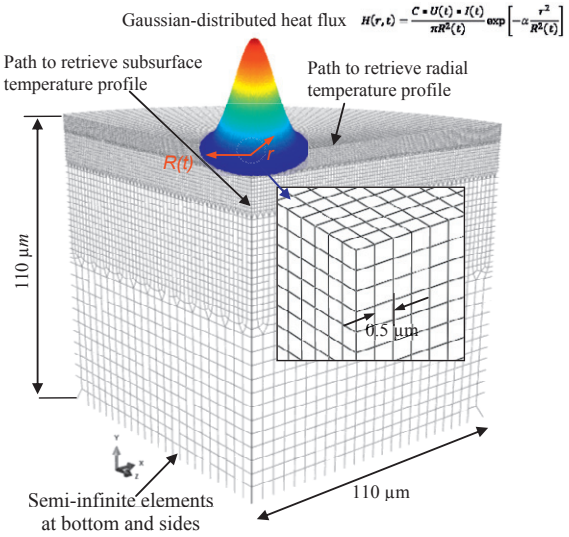

Fig. 1. 3D FEA mesh (quarter) with temporal and spatial Gaussian heat flux in single discharge EDM

2.3 Modeling of Gaussian distributed heat flux

The heat flux induced by EDM plasma is a function of discharge time and radial position. The heat flux obeys a Gaussian distribution, *H(r,t)* is given by

$$H(r,t) = \frac{C \bullet U(t) \bullet I(t)}{\pi R^2(t)} \exp\left[-m\frac{r^2}{R^2(t)}\right] \quad (1)$$

where *H(r,t)*: Time/-space dependent heat flux (W/m^2)
U(t): Time-dependent discharge voltage (V)
I(t): Time-dependent discharge current (A)
R(t): Time-dependent plasma radius (m)
r: Radial distance from the plasma center (m)
t: Discharge time (s)
C: Fraction of plasmas energy to the workpiece
m: Coefficient to tune the shape of Gaussian curve

The fraction of plasmas energy to the workpiece is 0.18 based on the calibrated data by DiBitonto [7]. The coefficient of Gaussian curve is $m = 2$ since it only slight changes the slopes the curve. The time-dependent plasma radius [12] can be determined by

$$R(t) = 0.0249 \times t^{0.75} \quad (2)$$

Coding the temporal and spatial heat flux is very challenging and a user heat flux subroutine is a must. The user subroutine DFLUX has been programmed to apply a non-uniform heat flux across the top surface. It worked by assigning local origins at the plasma center and then calculated the radial distance to each node surrounding this new origin from the equation of a circle as

$$r = \sqrt{\left(curcoord(i,x)\right)^2 + \left(curcoord(i,z)\right)^2} \quad (3)$$

where *curcoord(i,x)* and *curcoord(i,z)* are coordinates of the current node at each time increment in a simulation. The circular heat flux was applied on the top corner surface. Fig. 1 shows a representative Gaussian heat flux applied on the top surface.

2.4 Construction of discharge current function

As reported by Mukund et al. [8] and Eubank et al. [9] that when the discharge time in the nanosecond regime, heat flux becomes infinite. As defined in Eq. (1), $H_0(r,t)$ is defined as

$$H_0(r,t) = \frac{C \bullet U(t) \bullet I(t)}{\pi R^2(t)} \quad (4)$$

$$H_0(r,t) = \frac{C \bullet U(t) \bullet I(t)}{0.0249^2 \pi t^{1.5}} \quad (5)$$

When discharge starts, *U(t)* is not zero as shown in Fig. 2. If *I(t)* was also assumed to be a constant in the literature, $H_0(r,t)$ takes the limit of infinite when *t* approaches to zero, i.e.,

$$\lim_{t\to 0} H_0(r,t) = \infty \quad (6)$$

To avoid the issue of numerical singularity at nanosecond, discharge current *I(t)* in Fig. 2 is constructed by the following three functions.

$$I(t) = K_1\, t^n,\ t \in [0, T_1] \quad (7)$$
$$I(t) = K_2,\ t \in (T_1, T_e - T_2\,] \quad (8)$$
$$I(t) = K_3 t\ + b,\ t \in (T_e - T_2, T_e\,] \quad (9)$$

With the *I(t)* function in the initial discharge period [0, T_1], $H_0(r,t)$ can be simplified as

$$H_0(r,t) = \frac{C \bullet U(t) \bullet K_1 \bullet t^{n-1.5}}{0.0249^2 \pi} \quad (10)$$
$$\lim_{t\to 0} H_0(r,t) = 0 \quad (n > 1.5) \quad (11)$$

Eq. (11) means that heat flux is very small at the initial discharge period (in the nanosecond time domain). It is also physically sound since the discharge energy is actually very small at the initial discharge period. The determination of exponent n depends on the generator and the measured current signal, which could be a future study subject. In this study $n = 2$ was used.

The *I(t)* parameters K_1, K_2, K_3, and *b* can be determined by solving the boundary conditions of the *I(t)* curve in Fig. 2. Due to the very short time periods of signal rising and down, T_1 and T_2 are assumed to be 2.5% of the discharge duration T_e. The determined values of the *I(t)* parameters are listed in Table 3.

$$I(t) = 0, \quad t = 0 \quad (12)$$
$$I(t) = I, \quad t = T_1 \quad (13)$$
$$I(t) = I, \quad t = T_e - T_2 \quad (14)$$
$$I(t) = 0, \quad t = T_e \quad (15)$$

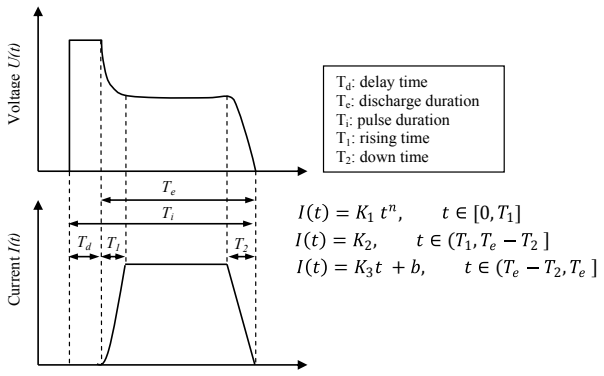

Fig. 2. Characterization of discharge voltage and current

3. Results and discussions

3.1 Evolutions of temperature and crater dimension

Figs. 3 and 4 show the temperature contours and craters at different discharge states under the concerned EDM conditions. At the end of initial discharge T_1 (1.25 μs), the peak temperature reaches to 8×10^5 °C in Fig. 3a, but the super high temperature (>10^5 °C) or superheating only spreads to a very small volume of material (radius 1.5 μm × depth 1.2 μm). Apparently numerical singularity is avoided using the constructed current functions at nanosecond discharge. Superheating would instantly vaporize the small volume of material. The gray zone (radius 5.55 μm × depth 5.0 μm) in Fig. 3b shows the volume of melted and vaporized material when its temperature is over the melting temperature 1353°C. At the middle of discharge duration $0.5T_e$ (25 μs), the peak temperature decreased to 8×10^4 °C in Fig. 3c. The very high temperature (>10^4 °C) spreads to a relatively large volume of material (radius 14 μm × depth 12 μm). The gray zone (radius 27.3 μm × depth 26.7 μm) in Fig. 3d shows the volume of melted and vaporized material. At the end of discharge duration T_e (50 μs), the peak temperature significantly decreased to only 3.4×10^3 °C in Fig. 3e since sufficient heat is conducted into the bulk material. The size of melted and vaporized material increases to radius 36.2 μm × depth 34.6 μm) in Fig. 3d.

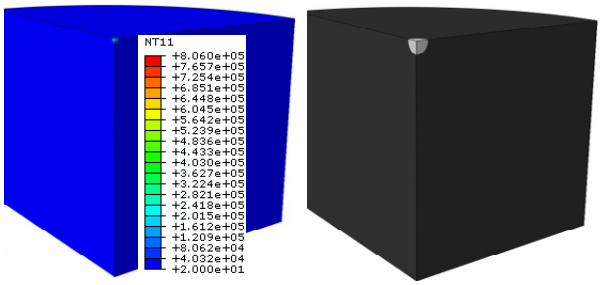

(a) Temp. contour @ T_1 (b) Melted material @ T_1

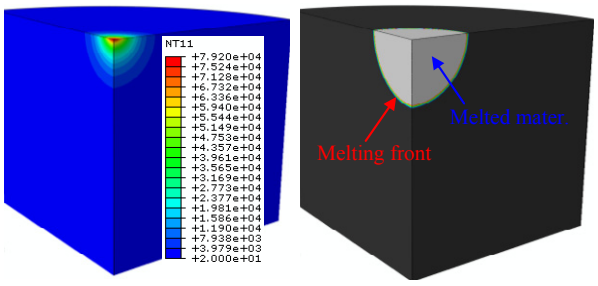

(c) Temp. contour @ $0.5T_e$ (d) Melted mater. @ $0.5T_e$

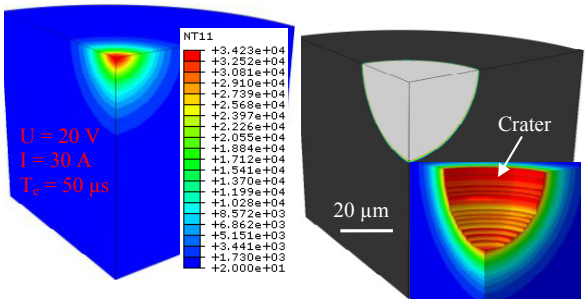

(e) Temp. contour @ T_e (f) Melted mater. @ T_e

Fig. 3. Representative temperature contour, melting front, and melted material at different discharge states

Fig. 4 shows the temperature profiles in radial and subsurface directions when the discharge time reduces from $0.5T_e$ to T_e. The temperature profiles in the subsurface have slightly higher gradients than those in radial direction. The temperature profiles also show the characteristics of Gaussian curves. The peak temperature varies in the range of 3.4×10^3 - 8×10^4 °C, which is on the similar order of 2×10^3 - 6×10^4 K reported by Eubank et al. [9]. In general, the peak temperature on the top surface significantly reduces, while the volume of melted and vaporized material increases when discharge time increases. The trend is also true for other EDM conditions. Apparently, superheating and melting are two sequential mechanisms for EDM erosion.

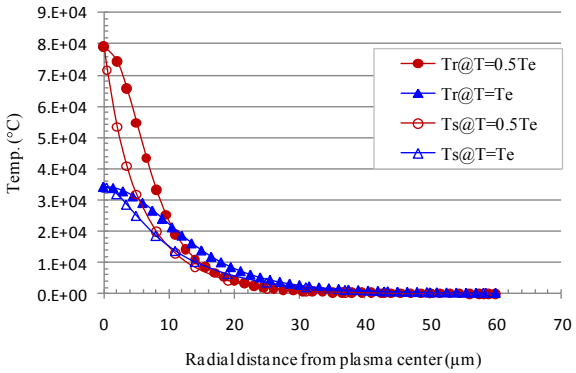

Fig. 4. Radial & subsurface temp. profiles at different discharge states

3.2 Effect of discharge duration and current on temperatures

The effects of discharge duration on radial and subsurface temperature profiles can be seen in Figs. 5 and 6. The range of discharge duration of 10 - 100 μs is within the normal variation of die sinking EDM. A decrease of radial and subsurface temperatures can be seen when the discharge duration increases. But a significant decrease occurs at the short discharge durations, the decrease becomes much less at the relatively long discharge durations. The peak temperature reduces from the order 10^5 °C to 10^4 °C when the discharge duration increases by 10 times. In addition, high temperatures penetrate much deeper and wider at short discharge durations than those at long discharge durations. Although a definition of superheating has not been defined in the literature, superheating may occur even at the longest discharge duration of 100 μs.

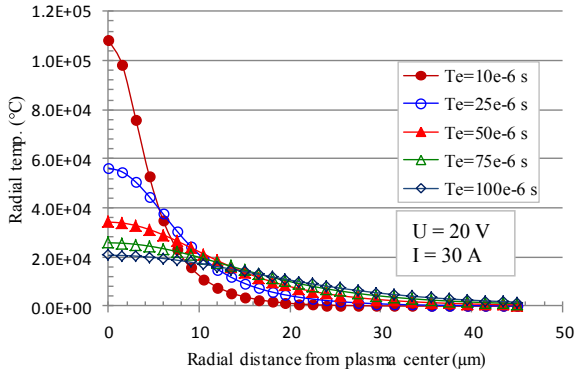

Fig. 5. Effect of discharge duration T_e on radial temperatures

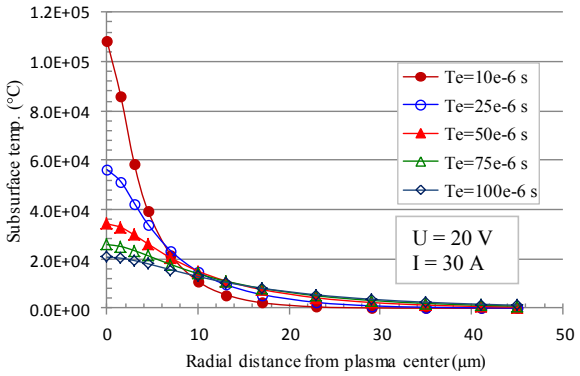

Fig. 6. Effect of discharge duration T_e on subsurface temperatures

Figs. 7 and 8 show the effects of discharge current on radial and subsurface temperature profiles. The peak temperature increases from 1.1×10^4 °C to 5.7×10^4 °C on the top surface when it increases from 10 A to 50 A. In contrast to the decreasing effect of discharge duration, discharge current has an even influence on temperature and its distributions. In other words, the influence of discharge duration on temperature is nonlinear, while the influence of discharge current is linear. Nevertheless, superheating and melting would happen sequentially in the simulated cases.

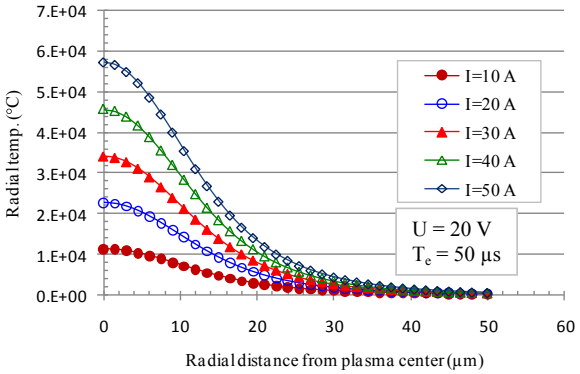

Fig. 7. Effect of discharge current I on radial temperatures

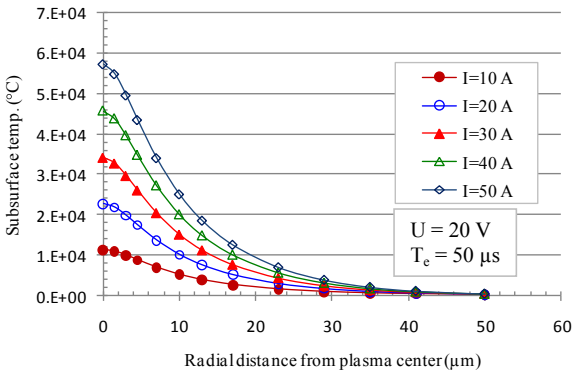

Fig. 8. Effect of discharge current I on subsurface temperatures

3.3 Effect of discharge duration and current on crater

The effects of discharge duration and current on crater radius and depth are shown in Figs. 9 and 10. It is expected that both the radius and depth of crater increase with the increase of discharge duration and current. The higher the discharge duration and current, the more discharge energy into the workpiece and more material erosion occurs.

It is interesting to note that the ratio of crater depth to radius decreases linearly from 0.99 to 0.92 when the discharge duration increases. It means that the melting front recedes due to the long time to allow re-solidification. In contrast, the ratio increases nonlinearly from 0.90 to 0.97 when the discharge current increases. It implies that the melting front advances due to high discharge energy to prevent re-solidification.

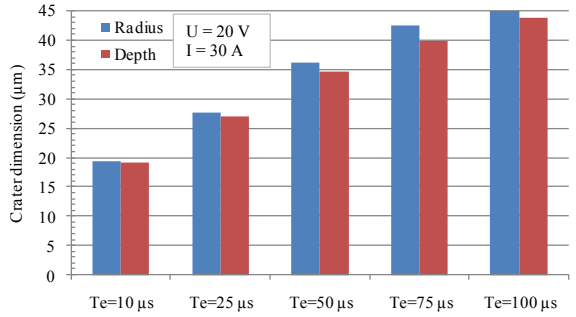

Fig. 9. Effects of discharge duration on crater dimensions

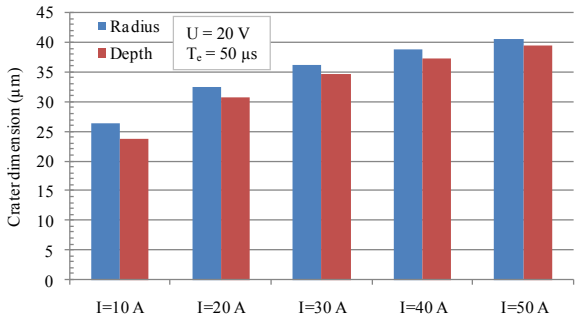

Fig. 10. Effects of discharge current on crater dimensions

The volume of crater was calculated by numerical integration of a melting front curve in each simulation case. Fig. 11 shows the effects of discharge duration and current on crater volume. The predicted increase of crater volume with discharge duration and current is simply due to the increased discharge energy.

It should be pointed out that the actual carter size should be smaller than the predicted one for two basic reasons. First, the vaporized material may be re-solidified into debris particles and or porous microstructures on an EDMed surface. Second, partial melted material can be splashed by EDM pressure and the rest melted material would be re-solidified into recast layer to from the crater bottom. However, a simulation of re-solidification of vaporized and melted material is beyond the scope of the study. Even though the discharge duration, current, and voltage are in the reasonable range, a comparison between the predictions and measured cater size and temperatures would not be made in the study since the simulation parameter values are not from an actual EDM experiment.

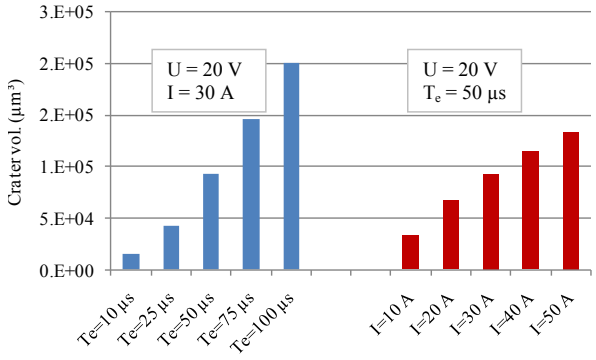

Fig. 11. Effects of discharge duration and current on crater volume

4. Discussions

The simulation work focused on a single EDM spark. Multiple-spark can also be simulated using the method if locations of multiple-sparks with time delays on the workpiece surface are known. However, the determination of random locations and time delays of multiple-spark are very challenging in an EDM experiment. In addition, the influence of convection on simulation prediction also needs further study.

5. Conclusions

A multiscale FEA simulation of single discharge EDM has been developed to understand the basic mechanisms of EDM erosion and process influence. The key findings are summarized as follows.

- The plasma-induced time/space-dependent Gaussian heat flux has been modeled and coded via a user subroutine in the FEA with convergence.
- The long-standing numerical singularity of heat flux in EDM modeling is solved, for the first time, using the innovative functions of discharge current.
- Peak surface temperature significantly decreases when discharge time increases, while the volume of melted and vaporized material increases.
- EDM temperature increases at longer discharge duration and higher current. However, the influence of discharge duration is nonlinear, while the influence of discharge current is linear.
- Melting front recedes at long discharge duration, while it advances at high discharge current.
- Superheating and melting are two sequential fundamental mechanisms for EDM erosion.

Acknowledgements

The authors would like to thank Alexander von Humboldt Stiftung/Foundation and NSF (Grant #1234696) for financial support of the collaborative research. Mr. Michael Sealy at the University of Alabama provided help in coding the user subroutine.

References

[1] Schumacher, B.M., 2004. After 60 years of EDM the discharge process remains still disputed, Journal of Materials Processing Technology, 149/1-3, pp. 376-381.
[2] Soldera, F., Lasagni, A., Mücklich, F., Kaiser, T., Hrastnik, K., 2005. Determination of the cathode erosion and temperature for the phases of high voltage discharges using FEM simulations, Computational Materials Science, 32/1, pp. 123-139.
[3] Marafona, J., Chousal, J.A.G., 2006. A finite element model of EDM based on the Joule effect, International Journal of Machine Tools and Manufacture, 46/6, pp. 595-602.
[4] Allen, P., Chen, X., 2007. Process simulation of micro electro-discharge machining on molybdenum, Journal of Materials Processing Technology, 186, pp. 346-355.
[5] Tan, P.C., Yeo, S.H, 2008. Modelling of overlapping craters in micro-electrical discharge machining, J. Phys. D: Appl. Phys., 41, p. 205302.
[6] Wang, Y., Bai, J., Guo, Y., Huang, H., Liu, J., 2010. Thermal modeling of the mateail removal rate of high-speed small hole EDM drilling using the computational fluid dynamics method, Proc. 16th Int. Sym. on Electromachining, pp. 705-710.
[7] DiBitonto, D.D., Eubank, P.T., Patel, M.R., Barrufet, M.A., 1989. Theoretical models of the electrical discharge machining process. I. A simple cathode erosion model, J. Appl. Phys., 66, pp. 4095-4103.
[8] Patel, M.R., Barrufet, M.A., Eubank, P.T., DiBitonto, D.D., 1989. Theoretical models of the electrical discharge machining process. II. The anode erosion model, J. Appl. Phys., 66, pp. 4104-4111.
[9] Eubank, P.T., Patel, M.R., Barrufet, M.A., Bozkurt, B., 1989. Theoretical models of the electrical discharge machining process. III. The variable mass, cylindrical plasma model," J. Appl. Phys., 73/11, pp. 7900-7909.
[10] Xia, H., Kunieda, M., Nishiwaki, N., 1996. Removal amount difference between anode and cathode in EDM process, IJEM, 1, pp. 45-52.
[11] SIMULIA, 2010, *Abaqus Standard*, ver. 6.10.
[12] Klocke, F., König, W., 2007. *Fertigungsverfahren 3: Abtragen, Generieren und Lasermaterialbearbeitung*, Spring-Verlag, Berlin, Heidelberg.